it is not presently known if this mechanism can explain the temperature dependence of the mobility in the intermediate temperature range. It has also been shown theoretically[24] that scattering by a two-phonon process could give a mobility temperature dependence similar to that observed in $SrTiO_3$ in the intermediate temperature range.

V. CONCLUSION

The electron Hall mobility has been measured from 1.5 to 550°K in reduced and niobium-doped $SrTiO_3$. Niobium appears to form a simple hydrogenic-type donor center in $SrTiO_3$ and consequently has a very small activation energy. The donor formed by the oxygen vacancy is doubly charged and has an activation energy of approximately 0.08 eV at low electron concentrations. The low-temperature electron mobility in niobium-doped $SrTiO_3$ is approximately a factor of 4 larger than in reduced $SrTiO_3$ over the electron-concentration range investigated. Low-temperature Hall mobilities as large as 2.2×10^4 cm²/V sec were measured in niobium-doped $SrTiO_3$. The measured electron mobility at low temperatures is approximately two orders of magnitude below the theoretical mobility for scattering by ionized defects. It is postulated that this discrepancy may be caused by a high concentration of compensated ionized defects. The high-temperature mobility has been analyzed in terms of scattering by polar optical lattice modes. The mobility behavior calculated from the known values of the electron-phonon coupling coefficients is not in agreement with the experimental results. However, the high-temperature mobility behavior can be approximated well by assuming scattering from a polar optical mode having a characteristic temperature of 600°K.

[24] B. W. Krishnamurthy and K. P. Sinha, J. Phys. Chem. Solids **26**, 1949 (1965).

ACKNOWLEDGMENTS

The authors wish to acknowledge the assistance of Mr. E. L. Stelzer in the experimental investigation and helpful discussions with Dr. D. Long and Dr. J. D. Zook.

PHYSICAL REVIEW VOLUME 155, NUMBER 3 15 MARCH 1967

Defects in Irradiated Silicon: Electron Paramagnetic Resonance and Electron-Nuclear Double Resonance of the Aluminum-Vacancy Pair

G. D. WATKINS
General Electric Research and Development Center, Schenectady, New York
(Received 12 September 1966)

An EPR spectrum produced in aluminum-doped silicon by 1.5-MeV electron irradiation is described. Labeled Si G9, it is identified as arising from an aluminum-vacancy pair, presumably formed when a mobile lattice vacancy is trapped by substitutional aluminum. The resonance is observed only upon illumination and is identified as a long-lived excited triplet ($S=1$) state of the defect. The observed hyperfine interactions with Al^{27} and neighboring Si^{29} nuclei, as well as the g tensor and axial fine-structure term D, are discussed in terms of a simple model of the defect using a linear combination of atomic orbitals. No Jahn-Teller distortion is observed in this excited state, as is consistent with the predictions of the model. Preferential alignment of the aluminum-vacancy axis direction in the lattice is achieved by stressing the crystal at ~200°C. The magnitude and sense of the alignment is consistent with the prediction of the model that the ground state is a Jahn-Teller distorted state similar to the phosphorus-vacancy pair previously studied. Abnormally strong $\Delta m\neq0$ nuclear hyperfine transitions are observed in the EPR spectrum, and the theory of this effect, found only in an even-spin system, is developed. Emission is observed for some of the lines in the spectrum similar to that reported by Tanimoto *et al.* for another photoexcited $S=1$ system. The origin of this effect is discussed in terms of the model.

I. INTRODUCTION

IN previous papers of this series,[1–5] we have shown that lattice vacancies in silicon produced by radiation damage are mobile at temperatures well below room temperature and can be trapped by impurities to form stable electrically active impurity-vacancy pairs. Examples are the oxygen-vacancy pair[1,2] (A center, giving the Si-B1 EPR resonance) and the phosphorus-vacancy pair[3] (E center, giving the Si-G8 resonance).

[1] G. D. Watkins and J. W. Corbett, Phys. Rev. **121**, 1001 (1961).
[2] J. W. Corbett, G. D. Watkins, R. M. Chrenko, and R. S. McDonald, Phys. Rev. **121**, 1015 (1961).
[3] G. D. Watkins and J. W. Corbett, Phys. Rev. **134**, A1359 (1964).
[4] G. D. Watkins, in *Proceedings of the 7th International Conference on the Physics of Semiconductors: Radiation Damage in Semiconductors* (Academic Press Inc., New York, 1965), p. 97.
[5] G. D. Watkins and J. W. Corbett, Phys. Rev. **138**, A543 (1965).

In this paper we report an EPR spectrum, labeled[4] Si-G9, that we interpret as resulting from a vacancy trapped by a substitutional aluminum atom. The arguments leading to this identification will be presented and a model of the electronic structure of the defect will be given that accounts for many of the features observed in the EPR and ENDOR studies. The resonance is observed only upon illumination at $\lesssim 20°$K, and we conclude that it results from an excited triplet ($S=1$) state.

Abnormally strong forbidden $\Delta m \neq 0$ nuclear hyperfine transitions are observed in the EPR spectrum, and in a separate section the theory for this effect, unique to an even-spin system, is developed.

II. EXPERIMENTAL PROCEDURE

Most of the experimental techniques have been described in previous publications.[1–5] The silicon samples were p type (aluminum $\approx 10^{15}$–10^{16}/cm^3) and were irradiated by 1.5-MeV electrons at room temperature or *in situ* in the microwave assembly at 20.4 or 4.2°K. Samples grown both by the floating-zone technique[6] and by pulling from a quartz crucible[7] were studied.

Most of the EPR studies were at 4.2°K in dispersion. At this temperature the relaxation times were long, and rapid passage effects[8] gave absorptionlike spectra 180° out of phase with respect to the modulation. The spectrum was studied both at 20 and 14 kMc/sec. ENDOR studies were performed by a technique previously described.[3] Light was introduced to the sample either through a hollow stainless-steel light pipe from outside the cryostat or by a light bulb in the microwave cavity assembly.

III. EXPERIMENTAL RESULTS AND ANALYSIS

A. EPR Spectrum

Figure 1 shows the observed spectrum at 14 kMc/sec in the presence of illumination at 4.2°K. For this orientation, ($\mathbf{H}\|\langle 112\rangle$), seven groups of lines can be observed, labeled a through g, which belong to this spectrum. (The six-line spectrum marked x will not concern us here. It has been labeled[4] G18 and is believed to arise from interstitial aluminum produced by the irradiation and will be discussed in a subsequent publication.) These groups spread over the full range of magnetic field available and versus crystalline orientation, their central positions are given in Fig. 2. The intensities of the lines vary with crystalline orientation, those shifting to high fields going through zero and reversing sign. This reversal is shown in Fig. 1 for g and is indicated in

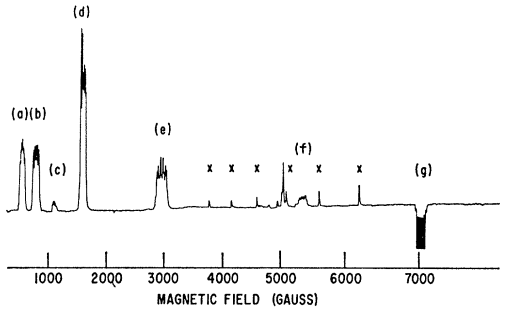

FIG. 1. The Si-G9 spectrum at 14 kMc/sec in the presence of illumination at 4.2°K, $\mathbf{H}\|\langle 112\rangle$. The seven groups of lines labeled a through g belong to the spectrum; those labeled x do not.

Fig. 2 by the dotted part of the curves. A discussion of the origin of this effect will be deferred to Sec. V.

The structure on each group of lines is complex but at a few specific magnetic field orientations the structure simplifies to six equally spaced, approximately equally intense lines plus weaker satellites. This is shown in Fig. 3 with $\mathbf{H}\|[211]$ for the group labeled d in Fig. 1. Upon rotation of the magnetic field away from the [211] axis, the structure splits out abruptly and becomes quite complex as indicated in Fig. 4. As an example, the structure after rotation by 30° (i.e., $\psi = 5.3°$ in Fig. 2) is shown in Fig. 5.

The positions of these groups of lines as well as the structure on each group can be fitted to the spin Hamiltonian

$$\mathcal{H}=\beta\mathbf{S}\cdot\mathbf{g}\cdot\mathbf{H}+D\{S_{z'}{}^2-\tfrac{1}{3}S(S+1)\}+\sum_j\{\mathbf{I}_j\cdot[\mathbf{A}_j\cdot\mathbf{S}-(\mu_j/I_j)\mathbf{H}]+\mathbf{I}_j\cdot\mathbf{Q}_j'\cdot\mathbf{I}_j\} \quad (1)$$

of a single defect species, with $S=1$ and with the axis of symmetry (Z') of the defect along a $\langle 111\rangle$ direction. The last terms are the nuclear hyperfine terms, the dominant interaction being with a single 100% abundant nucleus, $I=\frac{5}{2}$, which we identify as Al^{27}.[9] For it,

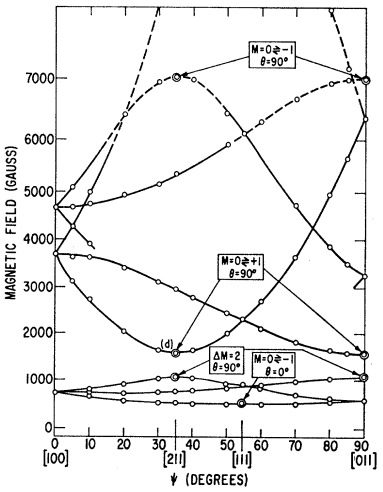

FIG. 2. Angular dependence of the spectrum observed at 14 kMc/sec. The dotted parts of the curves indicate the region in which the spectral lines are inverted.

[6] Obtained from General Electric Company Semiconductor Products Division, Syracuse, New York.

[7] Kindly supplied by Dr. R. O. Carlson.

[8] A. M. Portis, Phys. Rev. **100**, 1219 (1955); Sarah Mellon Scientific Radiation Laboratory, University of Pittsburgh, Technical note No. 1, 1955 (unpublished); M. Weger, Bell System Tech. **J. 39**, 1013 (1960).

[9] In the ENDOR results to follow, this identification will be verified.

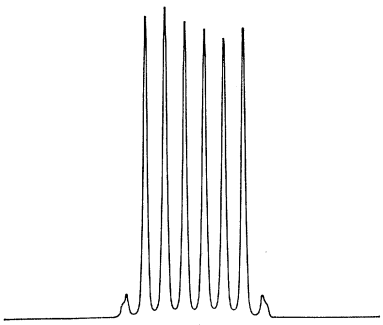

FIG. 3. Hyperfine structure associated with transition (*d*) in Fig. 1, $\mathbf{H}\|[211]$, $\nu_0=20$ kMc/sec.

both $\mathbf{A}_i$ and $\mathbf{Q}_i'$ are axially symmetric about the Z' axis. Also observed are hyperfine interactions with Si^{29} nuclei ($I=\frac{1}{2}$, 4.7% abundant) neighboring the defect. Taken together, the interactions will be shown to account for the structure observed on each group of lines.

The large excursions in the positions of the groups of lines arise because D is large, comparable to $g\beta H$. The several transitions observed arise from both the $\Delta M=1$ and $\Delta M=2$ transitions associated with each of the four differently oriented $\langle 111\rangle$ defects.

With the magnetic field along the axis of symmetry ($\theta=0°$), the wave functions are $|+1\rangle$, $|0\rangle$, and $|-1\rangle$, the eigenstates of S_z, and the allowed $\Delta M=1$, $\Delta m_j=0$ transitions are given to first order in $A_j/h\nu_0$, Q_j'/A_j, by

$$g_{\|}\beta H(M=0\rightarrow\pm 1)=h\nu_0\mp D-\sum_j m_jA_j. \tag{2}$$

With the magnetic field perpendicular to the axis of symmetry ($\theta=90°$), diagonalizing the secular determinant gives for the wave functions

$$\Psi_0=|0\rangle,$$
$$\Psi_{\pm 1}=\left\{\frac{1\pm\delta}{2}\right\}^{1/2}|+1\rangle\pm\frac{D}{|D|}\left\{\frac{1\mp\delta}{2}\right\}^{1/2}|-1\rangle, \tag{3}$$

where

$$\delta=(1+D^2/4g_\perp^2\beta^2H^2)^{-1/2}.$$

For this orientation, the three allowed $\Delta m_j=0$ transitions, to first order in $A_j/h\nu_0$, Q_j'/A_j, are given by

$$g_\perp\beta H(M=0\rightleftharpoons\pm 1)=|h\nu_0(h\nu_0\pm D)|^{1/2}-\sum_j m_jA_j,$$
$$g_\perp\beta H(M=-1\rightleftharpoons+1)=\tfrac{1}{2}|(h\nu_0)^2-D^2|^{1/2}-\sum_j m_jA_j. \tag{4}$$

For the Al^{27} nucleus, A_j is simply $A_{\|}$ in Eq. (2) and $A_\perp$ in Eq. (4). For the Si^{29} nuclei, whose axes do not coincide with the axis of the defect, A is given by the more general expression

$$g^2H^2A_j=\mathbf{H}\cdot\mathbf{g}\cdot\mathbf{A}_j\cdot\mathbf{g}\cdot\mathbf{H}. \tag{5}$$

Using Eqs. (2), (4), and (5), the analysis was performed on the groups of lines indicated in Fig. 2 by the double circles. Along the [011] and [211] directions, the three transitions are those of Eq. (4) for $\theta=90°$. Along the [111] direction, only one transition could be observed with $\theta=0°$, the other transition occurring at too high a magnetic field. Observations at both 14 and 20 kMc/sec were used in the analysis and the results for $\mathbf{g}$ and D are given in Fig. 6. (The sign of D cannot be determined by the analysis. The sign indicated in the figure is determined by considerations in later sections.)

For each of the groups of lines analyzed, $\theta=0°$ or 90°, and the hyperfine structure simplifies to the six-line pattern plus satellites shown in Fig. 3. The six-line structure we analyze as arising from hyperfine interaction with a single Al^{27} nucleus ($I=\frac{5}{2}$) giving

$$|A_{\|}|=(15.1\pm 0.1)\times 10^{-4}\ \text{cm}^{-1},$$
$$|A_\perp|=(15.6\pm 0.1)\times 10^{-4}\ \text{cm}^{-1}. \tag{6}$$

These values are fully consistent with the more accurate values given in the figure which were determined by ENDOR studies to be described in the next section.

The satellites in Fig. 3 we interpret as arising from hyperfine interaction with Si^{29} nuclei at three neighboring silicon atom sites. Their relative intensity is consistent with the assignment to three silicon sites, and from the angular dependence,[10] we conclude that the hyperfine constants are equivalent for each site but that their axes are different. The principal values and axes determined for these interactions are also given in Fig. 6.

The complexity of the hyperfine structure for orientations other than $\theta=0°$ or 90° arises from the emergence of "forbidden" $\Delta m_j\neq 0$ transitions. These transitions become allowed because of the large D term as has previously been pointed out by several authors.[11–13]

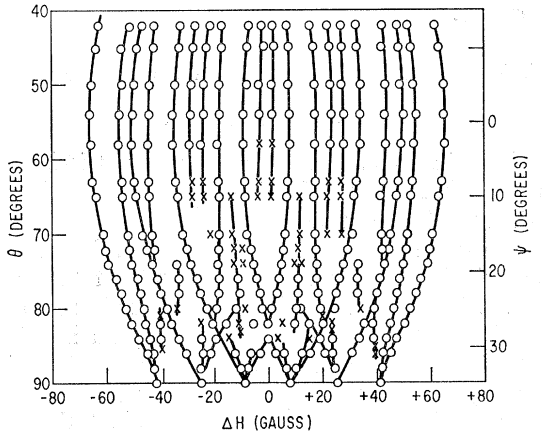

FIG. 4. Angular dependence of the hyperfine structure for transition (*d*) of Fig. 1, $\nu_0=20$ kMc/sec.

[10] The hyperfine structure is simple only for the magnetic field orientations used in the analysis. These serve to give three "windows" ($\mathbf{H}\|[211]$, [111], [011]), from which to unravel the Si^{29} angular dependence.

[11] J. Sierro, R. Lacroix, and K. A. Muller, Helv. Phys. Acta **32**, 286 (1959).

[12] G. W. Ludwig and H. H. Woodbury, Bull. Am. Phys. Soc. **5**, 158 (1960).

[13] B. Bleaney and R. S. Rubins, Proc. Roy. Soc. (London) **77**, 103 (1961).

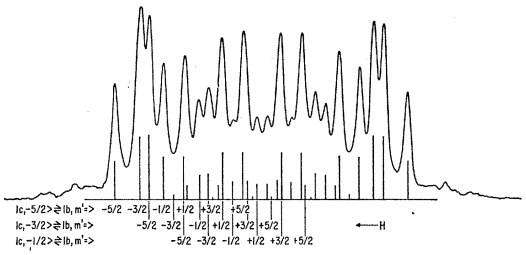

FIG. 5. Hyperfine structure for transition (*d*) of Fig. 1 for $\psi=5.3°$ (see Fig. 2), $\nu_0=20$ kMc/sec. Also shown is the calculated structure (see Sec. IV) assuming A positive and D negative.

However, the intensities observed for these transitions in this center are much larger than those considered by these authors and are a peculiar result of an even-spin system. These will be discussed in detail in Sec. IV.

B. ENDOR Spectrum

ENDOR studies of the Al^{27} hyperfine interaction were performed on the low-field $\Delta M=\pm1$ transitions for both $\theta=0°$ and $\theta=90°$. For $\theta=0°$, solution of Eq. (1) to first order in $Q'/h\nu_0$, $\mu H/Ih\nu_0$, and to second order in $A/h\nu_0$, gives the general expression for the ENDOR transitions

$$h\nu(M,\, m\rightleftarrows m-1)$$

$$=\Big|A_{\parallel}M-(\mu/I)H+\tfrac{3}{2}Q_{\parallel}'(2m-1)$$
$$-\frac{A_{\perp}^2}{2[(g_{\parallel}\beta H+2MD)^2-D^2]}$$
$$\times\{(g\beta H+2MD)[S(S+1)-M^2+(2m-1)M]$$
$$+D[S(S+1)-M^2](2m-1)+DM\}\Big|. \quad (7)$$

For our case of $S=1$, and with

$$h\nu_0=g\beta H+|D|$$

appropriate for the *low-field* $\Delta M=\pm1$ *transition*, Eq. (7) becomes

$$h\nu(0,\, m\rightleftarrows m-1)$$

$$=\Big|-(\mu/I)H+\tfrac{3}{2}Q_{\parallel}'(2m-1)$$
$$-\frac{A_{\perp}^2}{h\nu_0(h\nu_0-2|D|)}\{h\nu_0+|D|+(2m-1)D\}\Big| \quad (8)$$

and

$$h\nu(\pm1,\, m\rightleftarrows m-1)$$

$$=\Big|\pm A_{\parallel}-(\mu/I)H+\tfrac{3}{2}Q_{\parallel}'(2m-1)$$
$$-\frac{A_{\perp}^2}{2h\nu_0}\{\mp(2m-1)-1\}\Big|. \quad (9)$$

For $\theta=90°$, solving to the same order and using the wave functions of Eq. (3), we obtain for the ENDOR transitions associated with the *low-field* $\Delta M=\pm1$ *transition*

$$h\nu(0,\, m\rightleftarrows m-1)$$

$$=\Big|-(\mu/I)H+\tfrac{3}{2}Q_{\perp}'(2m-1)$$
$$+\frac{(A_{\parallel}+A_{\perp})^2\delta}{4h\nu_0(1-\delta|\epsilon|)}\{\epsilon(2m-1)-1\}\Big| \quad (10)$$

and

$$h\nu(\mp1,\, m\rightleftarrows m-1)$$

$$=\Big|\mp\delta A_{\perp}-(\mu/I)H+\tfrac{3}{2}Q_{\perp}'(2m-1)$$
$$-\frac{(A_{\parallel}+A_{\perp})^2}{8h\nu_0}(\delta\mp1)\mp\frac{A_{\perp}^2\delta^2\epsilon^2}{2h\nu_0}[\delta|\epsilon|+1]\Big|. \quad (11)$$

Here

$$\epsilon=D/2g\beta H$$

and

$$Q_{\parallel}'=-2Q_{\perp}'$$

consistent with $\mathrm{Tr}\mathbf{Q}'=0$. In Eqs. (9), (10), and (11) the upper sign is appropriate if D is positive, the lower if D is negative.

With these equations, the ENDOR transitions were analyzed to give the values of $\mathbf{A}$ and $\mathbf{Q}'$ given in Fig. 6. The analysis was facilitated by the knowledge that μ is positive. (All 100% abundant $I=\frac{5}{2}$ nuclei, of which

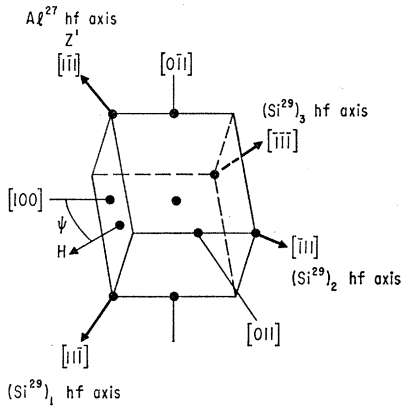

$g_{\parallel}=2.0136\pm.0003$

$g_{\perp}=2.0085\pm.0003$

$D=(-).4214\pm.0001\ \mathrm{cm}^{-1}$

Al^{27}: $A_{\parallel}=(+)15.152\pm.002(10^{-4}\ \mathrm{cm}^{-1})$; $A_{\perp}=(+)15.579\pm.003(10^{-4}\ \mathrm{cm}^{-1})$; $Q_{\parallel}'=(-).0144\pm.0006(10^{-4}\ \mathrm{cm}^{-1})$; $Q_{\perp}'=(+).0072\pm.0003(10^{-4}\ \mathrm{cm}^{-1})$

$Si^{29}_{1,2,3}$: $A_{\parallel}=\pm37.3\pm1.0(10^{-4}\ \mathrm{cm}^{-1})$; $A_{\perp}=\pm28.5\pm1.0(10^{-4}\ \mathrm{cm}^{-1})$

FIG. 6. Spin-Hamiltonian constants and relevant axes for one of the four equivalent defect orientations in the lattice.

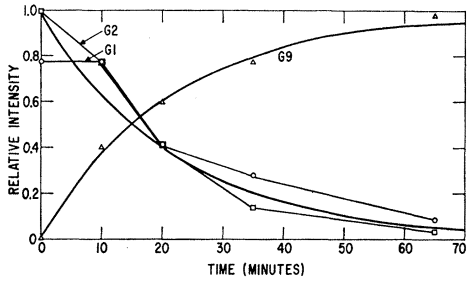

FIG. 7. Correlation of the growth of the G9 spectrum with the disappearance of the isolated vacancy spectra (G1 and G2) in an isothermal anneal at 170°K after a 20.4°K irradiation. The solid curves represent a best fit of a simple exponential decay and corresponding growth curve to the data. The ordinate gives the relative intensity of each spectrum, separately normalized.

there are only four, have positive magnetic moments.[14]) The analysis allows the determination of the relative signs of A and Q' with respect to D but not their absolute signs. The particular choice of signs given in Fig. 6 arises from considerations to be given in Sec. V.

From the $\theta=90°$ spectrum the value of μ was estimated to be $+3.644\pm0.003$ nm in close agreement with the Al^{27} value of $+3.6385$ determined by NMR.[14] No other element has a 100% abundant $I=\frac{5}{2}$ nucleus within this range and the identification with Al^{27} is thus verified. (The slight difference, though almost within experimental error, is probably real. Positive "chemical" shifts of the order of $\sim0.1\%$ would be consistent with the observed g shifts.[15])

C. Other Results

This spectrum is one of the dominant spectra produced by electron irradiation in aluminum-doped floating-zone silicon. It can be produced either by room-temperature irradiation or by warmup from a 20 or 4°K irradiation. It is not present directly after such a low-temperature irradiation but it appears upon annealing at ~170°K as the G1 and G2 spectra associated with the isolated vacancy[4,16] disappear. This is illustrated in Fig. 7 in an isothermal annealing study of this conversion. In this experiment the EPR observations were made at 4.2°K after each annealing interval. (All three spectra required illumination for observation, the G1 vacancy spectrum being optimized by globar light through an InAs filter, the G2 by tungsten light through a water filter, and the G9 spectrum by unfiltered tungsten light.) Throughout this conversion, the spectrum identified with interstitial aluminum ions[4] (see Fig. 1) does not appear to change in intensity.

In pulled silicon the spectrum is observed only very weakly. For instance, in one pulled crystal, doped with 10^{16} aluminum per cc, the room-temperature production rate of the spectrum was observed to be a factor of ~70 lower than in similarly doped floating-zone material. In this pulled crystal, the oxygen content was determined to be 7×10^{17} cm^{-3} from the intensity of the 9-μ absorption band associated with oxygen,[17] while that in the floating-zone crystal was below detectability, i.e., $\lesssim10^{16}$ cm^3.

The spectrum was not altered by the application of uniaxial stress *in situ* at 4.2 or 20.4°K. However, preferential alignment of the defects could be produced by the application of stress at ≈200°C. In this experiment a sample was stressed in an oven for 15 min at 200°C with 1700-kg/cm^2 compressional stress along a ⟨110⟩ direction. The sample was cooled to room temperature with the stress on, the sample then removed and placed in the cavity for 4.2°K observation. From the relative intensities of the multiplet groups of the spectrum, the members of the defects with their axes (Z') along each of the four ⟨111⟩ axes could be determined. It was found that a quenched-in alignment had occurred favoring the defects whose axes were perpendicular to the applied stress direction. The results are shown in Fig. 8, along with the disappearance of this alignment versus 15-min isochronal anneals.

In the same temperature region where the alignment disappears, annealing of the number of defects also occurs. The results of 15-min isochronal annealing of the spectrum intensity are also shown in Fig. 8.

In order to observe the spectrum, as mentioned before, it is necessary to illuminate the sample. Upon removing the light, the intensity is observed to decay at a rate which depends upon the transition involved, the orientation of the crystal, microwave power, etc. A detailed study of this has not been performed, but at 4.2°K the order of magnitude of this time constant is such that it varies from 2 to 10 sec.

IV. THEORY OF FORBIDDEN HYPERFINE TRANSITIONS

A. Perturbation Treatment

Sierro, Lacroix, and Muller,[11] Ludwig and Woodbury,[12] and Bleaney and Rubins[13] have pointed out that

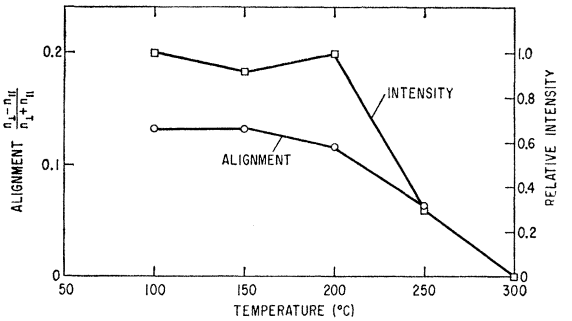

FIG. 8. Fifteen-minute isochronal-annealing study of the stress-induced alignment of the aluminum-vacancy axis, and the disappearance of the defect as monitored by the intensity of the spectrum.

[14] H. Kopfermann, *Nuclear Moments*, translated by E. E. Schneider (Academic Press Inc., New York, 1958).
[15] G. W. Ludwig and H. H. Woodbury, Phys. Rev. **117**, 1286 (1960).
[16] G. D. Watkins, J. Phys. Soc. Japan **18**, Suppl. II, 22 (1963).
[17] W. Kaiser and P. H. Keck, J. Appl. Phys. **28**, 882 (1957).

forbidden $\Delta m_j \neq 0$ hyperfine transitions become important in the presence of an axial fine-structure term D in the Hamiltonian. Following Bleaney and Rubins, consider the spin Hamiltonian

$$\mathcal{H}=g\beta\mathbf{H}\cdot\mathbf{S}+D\{S_{z'}{}^2-\tfrac{1}{3}S(S+1)\}+A\mathbf{S}\cdot\mathbf{I}-(\mu/I)\mathbf{H}\cdot\mathbf{I}. \quad (12)$$

Here, for simplicity, we consider the hyperfine interaction with only one nucleus and consider g and A to be isotropic.

It is instructive to consider the nuclear part of the Hamiltonian, which to first order in $A/g\beta H$ can be written

$$\mathcal{H}_N=\{A\langle\mathbf{S}\rangle-(\mu/I)\mathbf{H}\}\cdot\mathbf{I}=\{A\langle S_z\rangle-(\mu/I)H\}I_z+A\langle S_x\rangle I_x+A\langle S_y\rangle I_y. \quad (13)$$

In the absence of the D term, $\langle S_z\rangle=M$, $\langle S_x\rangle$ and $\langle S_y\rangle$ are zero, and the nucleus is quantized in the direction of the magnetic field (Z) for all electronic states $|M\rangle$. The eigenstates are thus $|M,m\rangle$ and the selection rules $\Delta M=\pm1$, $\Delta m=0$ are rigorously followed.

However, the presence of the D term produces nonvanishing values of $\langle S_x\rangle$ and $\langle S_y\rangle$. In particular, consider the Z' axis to be in the XZ plane and making an angle θ with the magnetic field (Z) direction, i.e.,

$$S_{z'}=S_z\cos\theta+S_y\sin\theta. \quad (14)$$

Solving the electronic part of the wave functions to first order in $D/g\beta H$, the expectation values of the components of $\mathbf{S}$ are, to first order in $D/g\beta H$,

$$\langle S_x\rangle\cong\frac{3}{2}\frac{AD\sin2\theta}{g\beta H}[M^2-\tfrac{1}{3}S(S+1)], \quad (15)$$

with $\langle S_y\rangle=0$ and $\langle S_z\rangle=M$. We see that the magnetic field seen by the nucleus is no longer strictly parallel to the external magnetic field direction but is tilted away, and by an amount which varies from one electronic eigenstate to another. As an electronic $\Delta M=\pm1$ transition occurs, therefore, the nuclear quantization axis changes and the nucleus may make a transition to any state in the new quantization system.

This physical picture can be made quantitative as follows: With (15), Eq. (13) becomes

$$\mathcal{H}_N\cong\{AM-(\mu/I)H\}I_z+\frac{3AD\sin2\theta}{4g\beta H}\times\{M^2-\tfrac{1}{3}S(S+1)\}\{I_++I_-\}. \quad (16)$$

This equation, expressed in the Z-axis system, manifests the "tilting" of the nuclear quantization axis by the presence of the I_+ and I_- terms which serve to mix the nuclear states $|m\rangle$.

Usually $|AM|\gg(\mu/I)H$, and for $M\neq0$, the nuclear states are separated in energy by $|AM|$. Solving the nuclear wave functions to first order in $D/g\beta H$, we get for the intensity of the $|M,m\rangle\leftrightarrow|M-1,\ m-1\rangle$ and $|M,\ m-1\rangle\leftrightarrow|M-1,\ m\rangle$ transitions

$$\sim\left(\frac{3D\sin2\theta}{4g\beta H}\right)^2\left\{1+\frac{S(S+1)}{3M(M-1)}\right\}^2\times\{I(I+1)-m^2+m\}, \quad (17)$$

where M, $M-1\neq0$. This is the result of Bleaney and Rubins and shows that the intensities of the forbidden $\Delta m=\pm1$ transitions are of the order of $(D/g\beta H)^2$. Transitions for $\Delta m=\pm2$, etc. also occur resulting from (16) and (15) carried to higher order in the perturbations. However, it will be sufficient to illustrate our point here to consider only the $\Delta m=\pm1$ transitions.

Equation (17) is not valid if M or $M-1=0$. This case does not arise for odd half-integral spins, for instance, with which Bleaney and Rubins were concerned. However, for an integral spin system such as ours, this case must also be considered.

For $M=0$, the nuclear energy states are separated only by $(\mu/I)H\ll A$ and the mixing by the off-diagonal terms of (16) becomes proportionately more important. For this case, the intensity of the $|M,m\rangle\leftrightarrow|M\pm1,\ m-1\rangle$ and $|M,\ m-1\rangle\leftrightarrow|M\pm1,\ m\rangle$ transitions is easily found to be

$$\sim\left(\frac{3D\sin2\theta}{4g\beta H}\right)^2\left(\frac{AI}{\mu H}\right)^2\left\{\frac{S(S+1)}{3}\right\}^2\times\{I(I+1)-m^2+m\}. \quad (18)$$

We see that the intensity is increased over the $M\neq0$ transitions by $\sim(AI/\mu H)^2$. This can be a very large number. In particular, for the Al^{27} hyperfine interactions in the spectrum of this paper, this quantity is ~50.

This enhanced effect for the $M=0$ state can be viewed as a result of the fact that the "tilting" of the field seen by the nucleus is much greater for this state. For this state, there is no field in the Z direction arising from the hyperfine coupling A and only the small applied field $\mathbf{H}$ remains. As a result, even a small value of $A\langle S_x\rangle$ in Eq. (13) can be very effective in tilting the nuclear hyperfine axis.

B. Calculation of the Structure

The perturbation treatment of the preceeding section served to give a qualitative feel for the magnitude of the effects and also gave some equations in the form necessary to augment the perturbation treatment of Bleaney and Rubins for future use by others. These formulas are not directly applicable to the spectrum considered in this paper, however, because D is not small with respect to $g\beta H$. In this section a more exact calculation will be outlined. We will calculate the structure for the low-field $\Delta M=\pm1$ transition, $\theta=60°$, $\nu_0=20$ kMc/sec, corresponding to the conditions of observation in Fig. 5 and a direct comparison to this observed structure will be made.

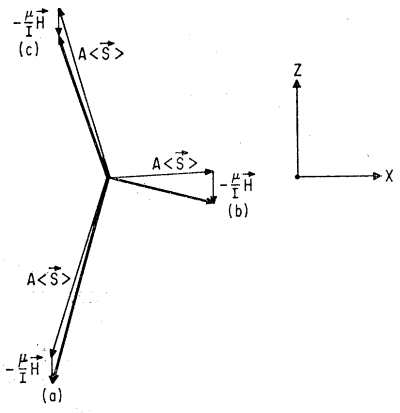

FIG. 9. Calculated nuclear quantization axes for each of the three electronic Zeeman states at $\theta=60°$, $\nu_0=20$ kmc/sec.

In this calculation, the Hamiltonian of Eq. (12) was used, the small quadrupolar interaction and the anisotropy in A and g being ignored. Straightforward diagonalization of the electronic part of the Hamiltonian [the first two terms of Eq. (12)], with $D/g\beta H=\pm 0.75$, gives for the wave functions

$$\begin{aligned}\Phi_a&=0.9732|\pm 1\rangle\pm 0.2013|0\rangle+0.1096|\mp 1\rangle,\\ \Phi_b&=-0.1705|\pm 1\rangle\pm 0.9555|0\rangle-0.2408|\mp 1\rangle,\\ \Phi_c&=-0.1530|\pm 1\rangle\pm 0.2157|0\rangle+0.9644|\mp 1\rangle,\end{aligned}\quad (19)$$

where the upper sign corresponds to positive D and the lower sign to negative D. The corresponding energy levels are given in Table I. Also given in the table are $\langle S_z\rangle$ and $\langle S_x\rangle$ determined directly from (19) for each state. Using these values with $A=\mp 15.4\times 10^{-4}$ cm^{-1} and $(\mu/I)H=2.22\times 10^{-4}$ cm^{-1}, the nuclear energy levels can be determined directly from Eq. (13). The predicted positions of the thirty-six $|c,m\rangle\leftrightarrow|b,m'\rangle$ possible transitions associated with the low-field $b\leftrightarrow c$ electronic transition follow directly and are indicated in Fig. 5 for A of opposite sign to D. The agreement is seen to be very good. (This agreement is not possible with A and D of the same sign, consistent with the opposite-sign assignment previously given in the ENDOR analysis.) (In the labeling of the states in the figure, m and m' are the azimuthal quantum numbers referred to the *nuclear* quantization axis for the b and c states, respectively, not the Z axis, i.e., external magnetic field direction. The signs indicated for m and m' are those consistent with negative D.)

In Fig. 9, we have plotted to scale $A\langle\mathbf{S}\rangle-(\mu/I)\mathbf{H}$ for each of the three states, using the values of $\langle S_z\rangle$ and $\langle S_x\rangle$ from Table I. This vector is proportional to the effective field seen by the nucleus, as seen by Eq. (13), and determines the nuclear quantization axis. This demonstrates vividly the large tilting of the hyperfine axes, particularly for the b state (which derives primarily from the $|0\rangle$ state). In the allowed $c\leftrightarrow b$ and $b\leftrightarrow a$ transitions therefore the almost 90° change in the nuclear axis assures that all nuclear transitions will become allowed.

In order to calculate the intensities of the transitions, the nuclear Hamiltonian, Eq. (13), was diagonalized and the wave functions determined for the six nuclear states of both the b and c electronic states. These wave functions, expressed as linear combinations of the nuclear states $|m\rangle$ (where the quantization axis is now the Z axis) allowed direct calculation of the intensities of the transitions as simply overlap matrix elements between the states.[18] The results are also indicated in Fig. 5, the intensities being indicated by the amplitudes of the predicted lines.

The agreement in Fig. 5 is seen to be very good. We conclude that the complex structure is indeed properly interpreted as arising from the "forbidden" nuclear transitions. We conclude that the origin is quantitatively understood in terms of the tilting of the nuclear hyperfine axis by the axial-field term D, with transitions to the $|0\rangle$ state of an even-spin system being particularly sensitive.

TABLE I. Calculated energies and spin components for the three electronic states at $\theta=60°$, $\nu_0=20$ kMc/sec.

State	$E/g\beta H$	$\langle S_z\rangle$	$\langle S_x\rangle$
a	± 1.0479	± 0.9352	± 0.3082
b	± 0.0794	∓ 0.0289	∓ 0.5557
c	∓ 1.1272	∓ 0.9067	± 0.2475

V. DISCUSSION

The correlation of the growth of the spectrum with the disappearance of the vacancy in Fig. 7 suggests that the defect is a lattice vacancy trapped by an aluminum atom. Consistent with this interpretation, we have previously shown[16] that the lattice vacancy executes long-range diffusional motion in p-type silicon in this temperature range. Also consistent with this interpretation is the role of oxygen in inhibiting the formation of the spectrum. Oxygen is known to be an effective trap for vacancies[1,2] and, in pulled crystals where the oxygen concentration is one to two orders of magnitude larger than the aluminum concentration, most of the vacancies would become trapped by the oxygen instead. Both substitutional aluminum atoms and interstitial ones (produced by the irradiation; see spectra labeled x in Fig. 1) might trap the vacancies. However, the failure to see significant diminution in the interstitial aluminum spectrum as the aluminum-vacancy pairs emerge would indicate that the aluminum-vacancy pair results

[18] A formally equivalent way of expressing the solution is in terms of the matrices $D^{5/2}(\alpha,\beta,\gamma)_{m'm}$, which describe how the eigenfunctions of angular-momentum $\frac{5}{2}$ transform under a rotation of coordinates. With β the angle between the nuclear hyperfine axes for the two electronic states (determined by solution of the electronic part of the problem), the intensity of the $m\rightleftarrows m'$ transition is given simply by $|D^{5/2}(0,\beta,0)_{m'm}|^2$. General expressions for these matrices are available. [See, for instance, M. Tinkham, *Group Theory and Quantum Mechanics* (McGraw-Hill Book Company, Inc., New York, 1964), p. 101ff.]

from the trapping of an isolated vacancy by a *substitutional* aluminum atom. (The high-temperature stability for the defect also argues against identification with an *interstitial* aluminum-vacancy pair since only one jump would be required to annihilate the defect reproducing substitutional aluminum.)

Because illumination is necessary to produce the spectrum, we do not know whether the charge state of the defect is the equilibrium state, or a metastable one, generated by the light. However, because the spectrum cannot be observed in the absence of light over a wide range of Fermi-level positions and because it disappears in ~10 sec after the light is turned off, even though the electronic equilibration times at 4.2°K are very long, we can conclude that the state being observed is an *excited* triplet state generated by the light. Presumably the ground state of this charge state is a singlet.

We thus tentatively conclude that the spectrum arises from an excited triplet $S=1$ state of some even-electron charged state of a vacancy trapped next to a substitutional aluminum atom.

A. Model

In Fig. 10, we show a simple one-electron linear-combination-of-atomic-orbitals (LCAO) molecular-orbital (MO) treatment of a lattice vacancy next to a substitutional aluminum atom. Here the atomic orbitals are the broken bonds (a,b,c,d) of the four correspondingly labeled atoms surrounding the vacancy. Atom c is an aluminum atom while the remaining three are silicon atoms. The point-group symmetry is C_{3V} and the one-electron LCAO molecular orbitals transforming according to the irreducible representations of this symmetry group are shown. Because the aluminum has one less nuclear charge than the silicon atoms, we anticipate that the (a_1'') orbital is elevated in energy as shown. The remaining (a_1') and (e) orbitals are expected to be closer together, with the completely symmetric (a_1') orbital probably lowest. By populating these one-electron orbitals, we now have a simple method of constructing an approximate many-electron wave function expected for the defect.

As mentioned before, we do not know the charge state involved but we do know that an *even* number of electrons are present in order to obtain $S=1$. It seems reasonable to assume therefore that there are either two (total charge $+1$) or four (total charge -1) electrons localized in these molecular orbitals. In general, the over-all two- or four-electron state could be $^3A_1$, $^3A_2$, or ^3E. We note however that no static Jahn-Teller distortion has occurred, the spectrum displaying the full axial symmetry of the aluminum-vacancy axis. We know from experience with other similar defects in irradiated silicon that if the state has orbital degeneracy, strong static Jahn-Teller distortions do take place. (See, for instance, the highly similar phosphorus-vacancy pair[3] which distorts from C_{3V} to C_{1h}.) We

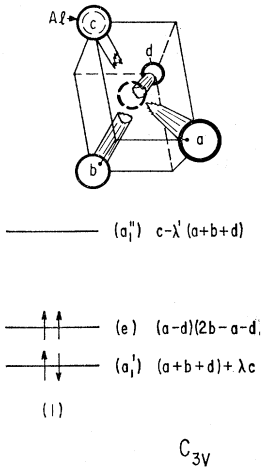

FIG. 10. Simple LCAO one-electron molecular orbital model for the electronic structure of the aluminum-vacancy pair. In this model, the excited electronic state seen in the resonance is the single minus $^3A_2$ state, made up primarily of the configuration shown, but with some admixture of higher $^3A_2$ configurations.

therefore tentatively[19] rule out the doubly degenerate ^3E state as a possibility and are left with the two orbital singlets $^3A_1$ or $^3A_2$.

In Table II, we list the configurational wave functions (for $S_z=S$) that give the $^3A_1$ and $^3A_2$ states. In this table the subscripts θ and ϵ refer to the two orthogonal (e) orbitals and the bars over the orbitals indicate spin down, the ones without bars indicating spin up. Each bracketed product wave function denotes a Slater determinant of two (or four) electrons distributed antisymmetrically between the two (or four) indicated one-electron states, respectively. We see that there is just one configuration possible in each case with the exception of the four-electron $^3A_2$ state for which there are three.

Since we are dealing with a long-lived excited state, we assume that we are dealing with the lowest-energy triplet state, the "bottleneck" for return to the ground state being the triplet-singlet transition. Since in both charge states the $^3A_1$ requires one electron in the elevated (a_1'') state, we anticipate that it is the highest in energy, and that the state seen in the resonance should be the $^3A_2$. We will see in the next section that the hyperfine analysis also indicates this state, the pre-

TABLE II. Configurational $^3A_1$ and $^3A_2$ wave functions ($S_z=+1$) for the aluminum-vacancy pair model of Fig. 10.

State	2 electrons		4 electrons
$^3A_1$	$(a_1'a_1'')$		$(a_1'a_1''e_\theta\bar{e}_\theta)+(a_1'a_1''e_\epsilon\bar{e}_\epsilon)$
$^3A_2$	$(e_\theta e_\epsilon)$	(1)	$(a_1'\bar{a}_1'e_\theta e_\epsilon)$
		(2)	$(a_1'\bar{a}_1''e_\theta e_\epsilon)-(\bar{a}_1'a_1''e_\theta e_\epsilon)$
		(3)	$(\bar{a}_1'a_1''e_\theta e_\epsilon)+(a_1'\bar{a}_1''e_\theta e_\epsilon)$ $-(a_1'a_1''\bar{e}_\theta e_\epsilon)-(a_1'a_1''e_\theta\bar{e}_\epsilon)$

[19] The possibility that the state is ^3E and that a *dynamic* Jahn-Teller distortion occurs still leaving an axially symmetric ground state must also be considered. We tested for this by applying uniaxial stress to the crystal, which should destroy the equivalence of the Jahn-Teller wells, and therefore induce departures from axial symmetry. The failure to see any such effects argues against this possibility.

TABLE III. Hyperfine parameters (a_j and b_j) and the corresponding molecular-wave-function coefficients (α_j^2, β_j^2, and η_j^2) calculated from the observed hyperfine structure.

Atom	Equiv. No.	a_j (10^{-4} cm^{-1})	b_j (10^{-4} cm^{-1})	$\alpha_j^2\eta_j^2$	$\beta_j^2\eta_j^2$	η_j^2
Si^{29}	3	(−)31.4	(−)2.9	0.023	0.087	0.11
Al^{27}	1	(+)15.294	(−)0.142	0.014	(0.006)	

dicted aluminum hyperfine interaction for the $^3A_1$ state being higher than that observed. We will also conclude that if this model is correct the charge state is probably the four-electron one, the configuration being primarily that labeled (1) in Table II, with small admixtures of (2) and (3). This is indicated in Fig. 10 by populating the relevant states with arrows, the sense of the arrows indicating the spin alignment.

B. Hyperfine Interactions

Following the procedure used for the analysis of previous centers,[1,3,5] we consider each of the one-electron wave functions for the unpaired electrons as linear combinations of atomic orbitals centered on the atoms near the defect.

$$\Psi_n=\sum \eta_{nj}\psi_j. \tag{20}$$

At each atom site j, we approximate ψ_j as a hybrid $3s3p$ orbital

$$\psi_j=\alpha_j(\psi_{3s})_j+\beta_j(\psi_{3p})_j, \tag{21}$$

where, for the atoms adjacent to the vacancy, we take the p function as directed approximately along the $\langle 111\rangle$ direction from the site to the center of the vacancy. To a good first approximation, the hyperfine interaction at the jth nuclear site is determined solely by ψ_j, i.e., that part of the wave function close to the nucleus. In this approximation, the hyperfine interaction is axially symmetric along the p-orbital axis and can be written

$$A_{\parallel}=a+2b, \tag{22}$$

$$A_{\perp}=a-b. \tag{23}$$

Here the isotropic term a arises from the Fermi contact interaction

$$a_j=\left(\frac{16\pi}{3}\right)(\mu_j/I_j)\beta\alpha_j^2\eta_j^2|\psi_{3s}(0)|_j^2, \tag{24}$$

where μ_j is the magnetic moment and I_j the spin of the jth nucleus. The anisotropic term b results from the dipole-dipole interaction averaged over the two-electron wave function and is given by

$$b_j=\tfrac{4}{5}(\mu_j/I_j)\beta\beta_j^2\eta_j^2\langle r_{3p}^{-3}\rangle_j. \tag{25}$$

In these equations η_j^2 is an average over the two one-electron orbitals involved in the $S=1$ state, i.e.,

$$\eta_j^2=\tfrac{1}{2}(\eta_{1j}^2+\eta_{2j}^2). \tag{26}$$

Using previously estimated[3] values for $|\psi_{3s}(0)|^2$ and $\langle r_{3p}^{-3}\rangle$ for both Al^{27} and Si^{29}, we can solve for the α_j^2, β_j^2, and η_j^2 associated with the principal hyperfine constants. The results are given in Table III.

Consider first the Si^{29} constants. Equations (24) and (25) predict that a_j and b_j should have the same sign as μ_j. With this assumption, there is no ambiguity in determining the a_j and b_j from (22) and (23) even though the absolute values of $A_{\parallel}$ and $A_{\perp}$ were not determined. (The signs in Table III are given in parentheses to indicate the fact that they were not determined experimentally.) We see that the atomic orbitals are 21% s and 79% p, similar to most of the other defects studied involving the dangling bonds around vacancies,[1,3,5,20] and that ~33% of the wave function can be accounted for in this manner on these three silicon sites. Comparing Fig. 6 to the model of Fig. 10, we identify these silicon sites as the a, b, and d sites neighboring the vacancy, with the three different $\langle 111\rangle$ hf axes of Fig. 6 corresponding to the three different atom-vacancy directions for the directed atomic orbitals.

The Al^{27} hf constants $A_{\parallel}$ and $A_{\perp}$ were determined to have the same signs from the ENDOR analysis leading to opposite signs for a and b. Clearly, the previous analysis, which predicts the same sign for a and b, is not valid here. However, ignoring this inconsistency for the moment and analyzing these constants in the same way, we see that the wave function appears to be mostly s-like and only ~2% of the wave function appears to be accounted for on the Al^{27}. This gives us a means of selecting between the $^3A_1$ and $^3A_2$ states (see Table II): In the $^3A_1$ configuration, the magnetic electrons would spend roughly as much time on the aluminum atom as on the three silicon atoms combined (via a_1''), giving ≈33%. However, the $^3A_2$ states with their magnetic electrons primarily in the (e) states, which have no admixtures of c, predict small interactions with the aluminum. We are therefore led to conclude that the spectrum is better explained by a $^3A_2$ state, consistent with the arguments of the previous section on energy considerations.

Although small, there is still a significant interaction at the aluminum site, and it remains to be explained. For the four-electron (−1) state, this could result from small admixtures of the excited $^3A_2$ configurations given in Table II. These serve to transfer spin density to the a_1' and a_1'' orbitals. (They are *excited* configurations because they involve promotion of an electron from the a_1' to the a_1'' state.) In this localized LCAO MO treatment, these effects are not present for the two-electron (+1) state and we are thus led to favor the identification with the four-electron (−1) state. (Similar effects can also occur for the +1 state if we include the "larger molecule" involving neighboring atoms and their electrons. We therefore cannot rule out this possibility. We

[20] G. D. Watkins and J. W. Corbett, Discussions Faraday Soc. 31, 86 (1961).

are inclined to feel however that the sizeable effects observed are more consistent with the relatively lower promotion energies to the excited-defect molecular-orbital states than those associated with the strong bonding silicon-silicon lattice atoms. In other words, the localized defect orbitals, because of their weaker overlap are much closer together in energy and are therefore considerably more polarizable.)

In general, by suitable admixtures of these excited $^3A_2$ configurations, either sign of spin density could be transferred to the aluminum atom. We argue, however, that a positive spin density is expected. This can be seen as follows: All of the molecular orbitals are made up from the *same* atomic orbitals on each atom. Since two electrons of the same spin state cannot coexist in a single atomic orbital, this is equivalent to a *repulsive* interaction between electrons of like spin. The driving force then to mix in the excited configurations is to spread the spin density over more sites, forcing the same sign of spin density over to the aluminum. Making this assumption, therefore, and using the fact that the magnetic moment of Al^{27} is positive, the isotropic hyperfine term a should be positive and is indicated as such in Table III.

Now consider the anisotropic b term for the Al^{27} interaction. In our simple treatment, the orbital on the aluminum might be expected to have p_σ character at least comparable to the s character (σ refers to the p function directed along the aluminum-vacancy axis), giving a positive b term and possibly an order of magnitude larger than that observed. Two possibilities might be considered for this discrepancy. In the first place, although no aluminum p_σ is allowed in the e orbitals by symmetry, p_π orbitals are. The admixture of the p_π orbitals (i.e., the wave functions admixing with part of the aluminum bonds to its silicon neighbors) would give a negative contribution to b. Secondly, of course, the c orbital on the aluminum could conceivably have much less p_σ character than that associated with the dangling silicon bonds to begin with. We have no *a priori* intuition in this regard. We recognize however that the bonds between the aluminum and its three silicon neighbors, because of the difference in nuclear charge, and with some partial ionic character, could depart from the usual $\sim sp^3$ tetrahedral bond admixture. For instance, if the aluminum moves into the vacancy and the bond angle to its neighbors closes, the fraction s in these bonds should decrease with a corresponding decrease in the p character of the dangling bond. (At 90°, for instance, simple directed valence concepts[21] predict pure p orbitals for the Al-Si bonds, leaving pure s for the dangling bond.)

The quadrupole interaction tells about the character of the *total* electronic charge-density distribution surrounding the aluminum nucleus and therefore also relates to this question. The quadrupole constant Q_{11}' is given by[22]

$$Q_{11}'=e^2qQ/2I(2I-1), \tag{27}$$

where eQ is the nuclear electric quadrupole moment and eq is the electric field gradient along the axis of symmetry at the nucleus. The field gradient strongly weights the charge density near the nucleus and can therefore be conveniently related to the unbalanced charge density in the $3p$ orbitals. Using the value $(e^2qQ)_{3p}=-12.516\times10^{-4}$ cm^{-1} determined from the measurements of Lew and Wessel[23] for the $^2P_{3/2}$ state of the neutral aluminum atom, we conclude that the magnitude of Q_{11}' indicates an unbalanced charge density along the aluminum-vacancy axis equivalent to 2.3% pure p. Assuming the value of a to be positive, Q_{11}' is negative which indicates an excess electronic charge density along the aluminum-vacancy axis.

This value of Q_{11}' is quite small and of opposite sign to what we might have expected. That is, in a simple view, an aluminum with an empty dangling bond pointing into a vacancy has a *deficient* electron density along the axis and of a magnitude corresponding to the fraction p_σ character in the bond. For an sp^3 bond this would be 75%. We note however that all of the effects previously mentioned—(1) the admixture of the other $^3A_2$ states (transferring charge density into the c orbital), (2) the admixture of p_π and e orbitals, (3) the partial ionic character of the Si-Al bonds (both transferring charge out of the aluminum p_π orbitals), and (4) the closing of the bond angles at the aluminum site to reduce the p_σ character in the b orbital—are equivalent to *increasing* the electronic charge density along the axis. Whether these effects are actually large enough to reduce the net quadrupole interaction to near zero and reverse its sign is difficult to say.

Taken together, the quadrupole interaction and the magnetic hyperfine interaction indicate that both the total charge density and the unpaired spin density in the valence shell of the aluminum depart only slightly from spherical (or cubic) symmetry. As we have indicated, this is a surprising result for an atom next to a vacancy. Although we have indicated mechanisms by which this might result, it is still surprising, and must be considered a serious challenge to the model of Fig. 10.

In view of this, let us consider briefly other possible models. It is possible that the aluminum atom may be farther from the vacancy, still along a ⟨111⟩ direction. However, in the silicon lattice, the nearest ⟨111⟩ substitutional site that is not a nearest neighbor (2.35 Å) is 7.05 Å distant, quite far removed. It is difficult to visualize why this particular aluminum-vacancy configuration should be stabilized when there are so many alternative ones closer that do not have ⟨111⟩ symmetry. It is possible to accommodate an *interstitial*

[21] L. Pauling, *The Nature of the Chemical Bond* (Cornell University Press, Ithaca, New York, 1948), 2nd ed., Chap. 3.

[22] T. P. Das and E. L. Hahn, *Nuclear Quadrupole Resonance Spectroscopy* (Academic Press Inc., New York, 1958), p. 17.

[23] H. Lew and G. Wessel, Phys. Rev. **90**, 1 (1953).

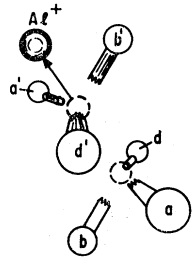

FIG. 11. Alternative model of the aluminum-vacancy pair in which the aluminum atom has "popped" backward into the on-axis interstitial site. Shown is a possible $^3A_2$ single plus charged state.

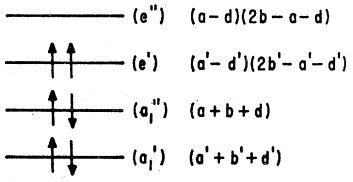

aluminum atom or ion close to the vacancy. Al^+ ($3s^2$), for instance, would show only small anisotropy. As noted before, it is hard to see however why an interstitial atom next to a single vacancy is stable up to ~200°C when a simple jump would annihilate the pair, producing substitutional aluminum.

One alternative model that deserves consideration is one in which the aluminum atom of Fig. 10 pops backward into the on-axis interstitial site. The resulting configuration can be viewed as an interstitial aluminum next to a divacancy and is illustrated schematically in Fig. 11. In the figure, admixtures between the two a_1 wave functions and between the two e wave functions have been omitted for simplicity as have admixtures of aluminum s and p_σ in the a_1 states and p_π in the e. The important point is that it is possible to arrive at a $^3A_2$ state which has a spin density distribution similar to that of Fig. 10. By this we mean that the unpaired electrons are in e orbitals primarily concentrated on the three silicon atoms around one of the two vacancies. Again configurational mixing plus exchange polarization of filled orbitals can produce the aluminum hyperfine interaction, but with a somewhat more natural explanation for the small anisotropy in the charge and spin density at the aluminum nucleus. We will not elaborate further on this model, which has its weaknesses too, but rather consider it in a more general sense as included in the model of Fig. 10, where the exact position of the aluminum atom along the axis is not well understood.

One further note is in order. Table III indicates that only about 35% of the wave function has so far been accounted for (33% on the three silicon atoms and 2% on the aluminum). This in turn might be interpreted to indicate that the remainder of the wave function is spread out over large distances surrounding the defect core. On the other hand, the arguments to be developed in the next section as to the origin of D indicate that the wave function is highly localized. The admixture of aluminum p_π into the e orbitals, previously discussed, represents a way out of this contradiction.

As an example, let us assume that the dangling bond at the aluminum remains an sp^3 orbital. The 1.4% s character, therefore, implies 4.2% of the wave function in p_σ. The observed anisotropy in the table on the other hand is equivalent to *missing* p_σ character of 0.6% implying 4.8% p_π in each of the two π orbitals. Adding these, we obtain 15% of the wave function on the aluminum (instead of 2%), giving ~48% of the wave function accounted for. This is beginning to approach the values (~60%) found for many of the other vacancy-related defects.[1,3,5,20] In fact, these numbers indicate that the total $3p$ character may be an order of magnitude greater than the $3s$. Under these circumstances, exchange polarization of inner cores by the $3p$ electrons can become important, causing an underestimate of the fraction $3s$. This would in turn scale up the total $3s$ and $3p$ concentration on the aluminum still further.

These arguments should be considered qualitative only. They do serve to show, however, that apparent "missing" spin density can be accounted for by distributing the wave function symmetrically among the $3p$ orbitals around an atom or of course into higher ($n=4$, 5, etc.) atomic states. This serves to strengthen the arguments about the role of the p_π orbitals. The total concentration of wave function on the aluminum therefore does not follow simply from the observed hyperfine interactions and because of this no estimate is made in Table III.

C. g and D

According to the model of Fig. 10, the two electrons are primarily in the e orbitals and the $^3A_2$ wave function can be approximated by

$$(2\sqrt{6})^{-1}\{(a-d)_1(2b-a-d)_2 - (2b-a-d)_1(a-d)_2\}\chi^+, \quad (28)$$

where χ^+ is the symmetric $S=1$ spin function. One source of the D term is the magnetic dipole-dipole interaction between the two electrons. Averaging this over the wave function given by Eq. (28), ignoring overlap terms, we estimate D from this source to be $\sim+2\times10^{-2}$ cm^{-1}. This is more than an order of magnitude below the observed value (and of opposite sign if the assumed sign of a for Al^{27} is correct), and we conclude that this is probably not the dominant source of D.

If the electrostatic interactions between the electrons are strong, as we might expect for a highly localized wave function, D can arise through spin-orbit interaction. For instance, in the case of a single atom or ion where the strong electrostatic interactions between electrons give rise to Russell-Saunders coupling, the spin-orbit interaction can be written $\lambda\mathbf{L}\cdot\mathbf{S}$ and the $\mathbf{g}$ and $\mathbf{D}$ tensors are given by[24]

$$\mathbf{g}=2(1-\lambda\mathbf{\Lambda}),$$
$$\mathbf{D}=\lambda^2\mathbf{\Lambda},$$

[24] M. H. L. Pryce, Proc. Phys. Soc. (London) A63, 25 (1950).

where **A** is given by a sum of matrix elements of orbital angular momentum to excited atomic states within the same atomic term (same **L** and **S**). We note the relationship between **D** and the g shift

$$D_{ij}=\tfrac{1}{2}\lambda\Delta g_{ij}. \quad (29)$$

Even though the defect wave function of concern to us is a molecular one, the spin-orbit interaction is of atomic origin, at each of the atom cores, and the treatment above for the single atom continues to have some relevance.[25] Equation (29) therefore serves to give us a rough estimate of the spin-orbit contribution to D. With $\lambda=-0.02$ eV (the magnitude is that for atomic silicon[26]; the sign comes from the fact that the g shifts are positive), and with $g_{\parallel}-g_{\perp}=+0.0051$, Eq. (29) gives

$$D=D_{\parallel}-D_{\perp}\simeq-0.4\ \text{cm}^{-1}.$$

Both the sign and order of magnitude agree with the observed value. (The agreement is actually very close, but this must be considered fortuitous.) We therefore conclude that the large D term observed in the spectrum originates via the spin-orbit interaction. The predicted negative sign gives further support to the assignment of the signs in Fig. 6.

The relative magnitudes of the g shifts and their signs appear reasonable in terms of the model in Fig. 10. In particular, we have previously shown[3] that the g shift associated with an electron in a single dangling silicon bond is $\Delta g_{\parallel}'\sim 0$, $\Delta g_{\perp}'\sim+0.01-0.02$, where "parallel" and "perpendicular" refer to the dangling-bond axis. Ignoring the interactions between spins, these one-electron contributions averaged over the wave function of Eq. (29) predict positive g shifts of the correct magnitude with $\Delta g_{\parallel}/\Delta g_{\perp}=8/5$, in close agreement with the observed ratio 1.82.

These arguments as to the origin and predicted magnitudes of **g** and **D** are primarily qualitative ones and are meant only to indicate that the observed values are reasonable in terms of the model. A quantitative treatment would be a formidable task and is beyond the scope of this paper.

D. Inversion of the Spectral Lines

As indicated in Figs. 1 and 2, some of the spectral lines are inverted. Tanimoto, Ziniker, and Kemp[27] have observed similar effects in a photoexcited triplet state of an axially symmetric defect in CaO. They explained

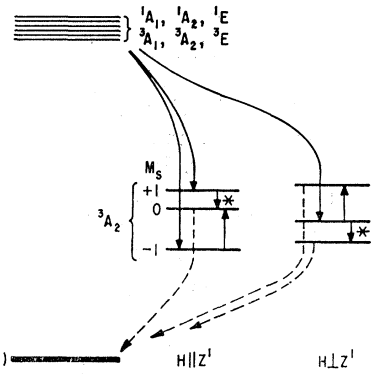

FIG. 12. Schematic model for the inversion of the high-field spectral lines. Both selective optical pumping and selective depopulation to the ground state are considered. The emissive transitions are indicated with an asterisk.

the effect as a level inversion resulting from selective generation of either the $M=0$ or $M=\pm1$ states over the other. They interpreted the mechanism as resulting from the anisotropic spin-orbit coupling in the optically excited states (resulting from the axially symmetric crystalline field), and its role in the selection rules for the singlet-triplet transition.

In Fig. 12, we incorporate their interpretation to the conditions of the aluminum-vacancy pair. As mentioned before, the spin-orbit interaction originates near the silicon-atom cores. At these sites the "crystalline field" associated with the vacancy is along the ⟨111⟩ axis pointing toward the vacancy. This field is effective in quenching the orbital angular momentum perpendicular to this direction but still allows orbital moments to be generated in excited atomic states along the direction. Averaging over the three silicon sites, we conclude that the spin-orbit interaction in excited electronic states should be anisotropic with a smaller value parallel to the vacancy-aluminum axis than perpendicular to it.

So long as the crystal-field splittings are large compared to the singlet-triplet spacings in the excited states, it follows also that the coupling via spin-orbit interaction between the excited singlet and triplet states will reflect this same anisotropy.

This coupling mixes the singlet and triplet states allowing direct optical excitation to the triplet state. Alternatively, excitation to a singlet state followed by a singlet-triplet transition via lattice modulated spin-orbit coupling can also populate the triplet state. In either case the low spin-orbit coupling along the defect axis will cause the $\Delta S_z'=\pm1$ transitions to dominate. With $\mathbf{H}\|Z'$, this gives preferential generation of the $M=\pm1$ states while with $\mathbf{H}\perp Z'$, the $M=0$ state is preferentially generated. This is shown in Fig. 12, with the resulting emissive transitions (the high-field ones) shown by an asterisk.

In order to see these level inversions, it is necessary that the spin-lattice relaxation time be comparable to or longer than the triplet lifetime itself. This means that

[25] In general, it is always possible to replace the spin-orbit interaction by $\lambda\mathbf{L}\cdot\mathbf{S}$ in dealing with a matrix element between states of the same **L** and **S**. This holds in particular for the relevant matrix elements to other triplet states. This does not account properly for matrix elements to singlet states, however, which are probably also important.

[26] Two-thirds the energy difference between the $P_{3/2}$ and $P_{1/2}$ levels of neutral silicon as given in *Atomic Energy Levels*, Natl. Bur. Std. (U.S.) Circ. No. 467 (U. S. Government Publishing and Printing Office, Washington, D. C., 1949).

[27] H. Tanimoto, W. M. Ziniker, and J. O. Kemp, Phys. Rev. Letters **14**, 645 (1965).

the selection rules for the return to the ground singlet must also be considered. Although this was not considered by Tanimoto *et al.*, it is easy to show that in our case these selection rules should be just the reverse of those for the generation and therefore have the same effect on the populations. In particular, the $^3A_2$ state observed in the resonance is made up of atomic orbitals of p_σ character which have their orbital moments *quenched along* the silicon-vacancy axis. The anisotropy of the spin-orbit coupling for this state is therefore reversed and admixtures of singlet into this state (which make the transition allowed to the ground state) cause the reverse selection rule. These transitions are also indicated in Fig. 12.

The selective transitions out of the triplet state give a mechanism for level inversion in the absence of anisotropic generation. In particular, the triplet state could be generated by capture of an electron or hole from the conduction or valence bands—not a localized excitation—and in that case uniform generation of all states might be expected. We do not know the mechanism of generation in our case but the fact that light of energy in the vicinity of the band gap is most effective suggests that this may be the mechanism of generation.

In our case the high-field lines are inverted while Tanimoto *et al.* found the low-field lines inverted. We have interpreted the sign of D for both defect systems to be negative. The difference arises from the fact that in their case the crystal-field axis which determined the anisotropy of the spin-orbit interaction was parallel to the defect axis and the selection rules were reversed from those here.

E. Stress Alignment

The quenched-in alignment produced by stress at elevated temperatures (~200°C) will reflect the properties of the stable charge and electronic state of the defect at that temperature. The $^3A_2$ electronic state indicated by Fig. 10 for the photoexcited triplet state can be expected to have little bearing on the response of the defect to stress at these elevated temperatures. Although we have no direct way of determining the ground electronic state at these temperatures we can make an intelligent guess.

Referring to the one-electron orbitals of Fig. 10, we would expect the configuration to be $(a_1')^2e^2$ for the four-electron (−1) state and $(a_1')^2e$ for the three-electron (neutral) state. The corresponding available states are ^1E, $^3A_2$, and $^1A_1$ for the minus state and ^2E for the neutral. Because a Jahn-Teller distortion can take place for the degenerate E states and thereby lower their energy, we anticipate that this state is favored in both cases.

This argument probably applies even for the two-electron (+1) state. The $(a_1')^2$ state gives $^1A_1$, but a ^1E state is available from the slightly higher energy configuration $a_1'e$. From previous experience, we know that the Jahn-Teller energies can be large with respect to the a_1'-e separation[28] and we therefore conclude that here too the Jahn-Teller distorted ^1E state is probably lowest.

In each of these charge states we therefore argue that the lowest-energy state is a Jahn-Teller distorted E state. The defect therefore becomes formally similar to the phosphorus-vacancy pair, a ^2E state in C_{3v}, which has been studied extensively in resonance.[3] There it was found that the Jahn-Teller distortion was one of e symmetry with two of the three silicon atoms pulling together in a pair-wise bond and lowering the local symmetry to C_{1h}.

It is therefore instructive to compare the stress-induced alignment achieved for the Al-vacancy pair with that previously reported for the phosphorus-vacancy pair. For the phosphorus-vacancy pair, 1800-kg/cm² stress along a ⟨110⟩ axis at 300°K gave $n_\perp/n_{||}=1.75$, where $n_\perp$ denotes the number of defects with phosphorus-vacancy axes perpendicular to the ⟨110⟩ stress direction, and $n_{||}$ denotes the number with axes along the other ⟨111⟩ axes. To compare this to the aluminum-vacancy stress studies at ~190°C and 1700 kg/cm², it is desirable to scale the appropriate stress-induced Boltzmann weightings of the different orientations to the same stress and temperature. Following the method outlined in the paper on the vacancy-phosphorus pair[3] the 1.75 factor would be expected to correspond to a value of 1.39 if the phosphorus-vacancy pair alignment were that associated with the quenched-in equilibrium for 1700-kg/cm² stress at 190°C. This is very close to the value 1.33 observed in Fig. 8 for the aluminum-vacancy pair.

For the phosphorus-vacancy pair we concluded that the alignment was in large part a manifestation of the coupling between the Jahn-Teller distortion and the applied strain. The similar alignment for the aluminum-vacancy pair gives support to the speculation that its ground state is also a Jahn-Teller distorted E state.[29]

As noted for the phosphorus-vacancy pair,[3] the reorientation of the defect given[30] in Fig. 10 requires that the vacancy make two diffusional jumps away from the aluminum (or phosphorus) and then return. The activation energy for reorientation thus includes a term arising from the binding energy between the vacancy and the impurity. The fact that reorientation requires a temperature ~200°C higher for the aluminum-vacancy pair indicates a substantially higher binding energy for it. On the other hand, the disappearance of the defect in the same temperature range indicates that the remaining binding at the next-next nearest site is small.

[28] The strong admixture of e and a_1 orbitals upon distortion found for the phosphorus-vacancy pair (see Ref. 3) indicates this.

[29] Similar arguments could have been made throughout for the model of Fig. 11. Here the formal similarity is with the divacancy (see Ref. 5), which is also a Jahn-Teller distorted E state with comparable stress-induced alignment.

[30] The arguments of this paragraph may not apply to the model of Fig. 11. The motion for its reorientation is less obvious.

VI. SUMMARY AND CONCLUSIONS

We conclude that the G-9 spectrum described in this paper arises from the photoexcited triplet ($S=1$) state of an aluminum-vacancy pair. It is apparently formed when a mobile lattice vacancy, produced by radiation damage in the lattice, is trapped by a substitutional aluminum atom. Consistent with this interpretation, the production of this center is greatly reduced in pulled crystals, containing $\sim 10^{17}$–10^{18} cm^{-3} oxygen, the oxygen in that case serving as the dominant vacancy trap.

A microscopic model has been presented for the defect and the electronic structure has been described in terms of one-electron LCAO molecular orbitals associated with the four lattice atoms surrounding the vacancy, one of which is the aluminum. In this model, the resonant state is identified as $^3A_2$ (of C_{3v}), with a sizeable fraction of the unpaired spin density on the three silicon atoms, consistent with the observed hyperfine interactions with these nuclei. Configurational interaction with higher $^3A_2$ states is called upon to explain the isotropic part of the observed hyperfine interaction with the aluminum. The charge state of the defect could be either $+1$ or -1, but the strength of the aluminum hyperfine interaction is best explained if the charge state is -1.

The near-isotropic hyperfine interaction with the aluminum and its small quadrupole interaction are somewhat surprising in terms of the model. A number of possible causes have been considered. Among these is the possibility that the aluminum atom is displaced either inward toward the vacancy or backwards into the on-axis interstitial position. It is concluded that the position of the aluminum atom remains somewhat in doubt. Also considered important in this regard is the admixture of aluminum p_π orbitals into the $^3A_2$ state.

From the LCAO molecular model, it is argued that the ground state of the defect is probably a Jahn-Teller distorted E state similar to that of the phosphorus-vacancy pair previously studied. The similar behavior under uniaxial stress at elevated temperature for the two defects is consistent with this conclusion.

Lattice vacancies therefore interact and form stable electrically active defect pairs with a rich variety of point defects. We have previously shown that they interact with substitutional group-V *donors* (with phosphorus to form the E center), with *electrically inactive* impurities (with interstitial oxygen to form the A center), and with *other vacancies* to form divacancies. In this paper we show that they also pair with substitutional group-III *acceptors*. This dual role of interacting with both donors and acceptors is consistent with the discovery[4] that the lattice vacancy can act as either acceptor in n-type material or donor in p-type. In both cases the interaction might be viewed as a result of Coulomb attraction between donors and acceptors, where the vacancy plays the appropriate role of acceptor in n-type and donor in p-type material.

ACKNOWLEDGMENTS

It is a pleasure to acknowledge the assistance of W. Colliton in all phases of the measurements. G. Ludwig and H. H. Woodbury kindly made their spectrometer available for the 14-kMc/sec studies and C. R. Trzaskos assisted in these measurements. Helpful discussions with F. S. Ham and J. W. Corbett are gratefully acknowledged.